Electronic Supplementary Material (ESI) for Materials Advances.

Supplementary Material: Molecular Dynamics Investigation of the Structural and Energetic Properties of CeO_2-MO_x (M = Gd, La, Ce, Zr) Nanoparticles

João Paulo A. de Mendonça,[*,†] Tuanan C. Lourenço,[*,†] Luis Paulo M. Freitas,[*,‡] Anderson A. E. Santo,[*,‡] Gustavo T. Feliciano,[*,‡] and Juarez L. F. Da. Silva[*,†]

†*São Carlos Institute of Chemistry, University of São Paulo, PO Box* 780*,* 13560-970*, São Carlos, SP, Brazil*

‡*Institute of Chemistry, São Paulo State University, PO Box* 55*,* 14800-900*, Araraquara, São Paulo, Brazil*

E-mail: jpalastus@gmail.com; lourenco.tuanan@gmail.com; luispaulomezzinafreitas@gmail.com; anderson.santo@unesp.br; gtfeliciano@gmail.com; juarez_dasilva@iqsc.usp.br

Contents

1 Introduction

The nanoparticles were generated by the ammorphisation/recrystalization approach based on the works published by Sayle's group along the years.[1,2] Here, we included the tests performed along the work, the optimized final nanoparticle generation approach and the results omitted in the main paper for simplicity and easy reading.

2 Ammorphisation

2.1 Pristine Crystal Construction and Relaxation

Our first step was to reproduce the ammorphisation/recrystalization process from Sayle and Parker works[3] and build a cubic CeO_2 nanostructure using a simple Buckingham model (without the charge polarization) in LAMMPS. A specific approach was developed based in the information from the Sayle and Parker papers.

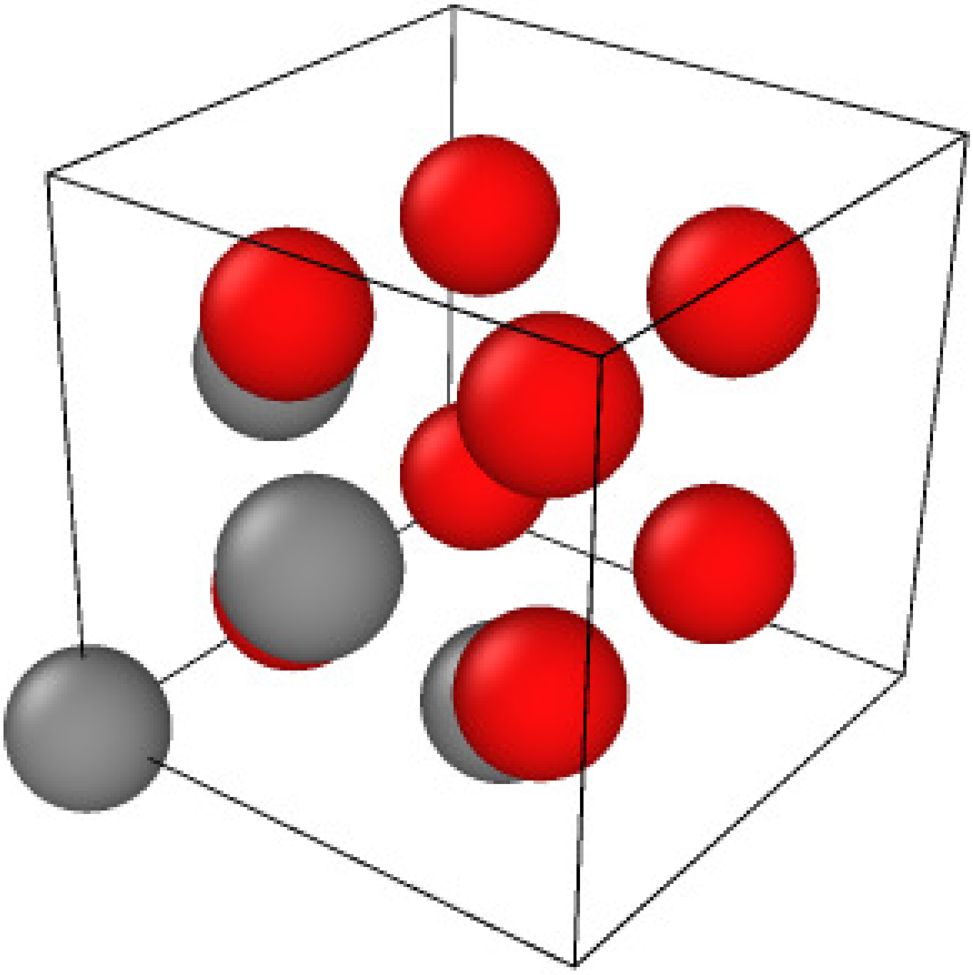

Figure S1: Visualization of the cell extracted from the original CIF file and used to build the initial box configurations/supercells.

First, the CIF with the computed structure for CeO_2 was downloaded from COD,[4,5] Figure S1, and a 6 × 6 × 6 supercell containing 2592 atoms was built using LAMMPS, Figure S2.

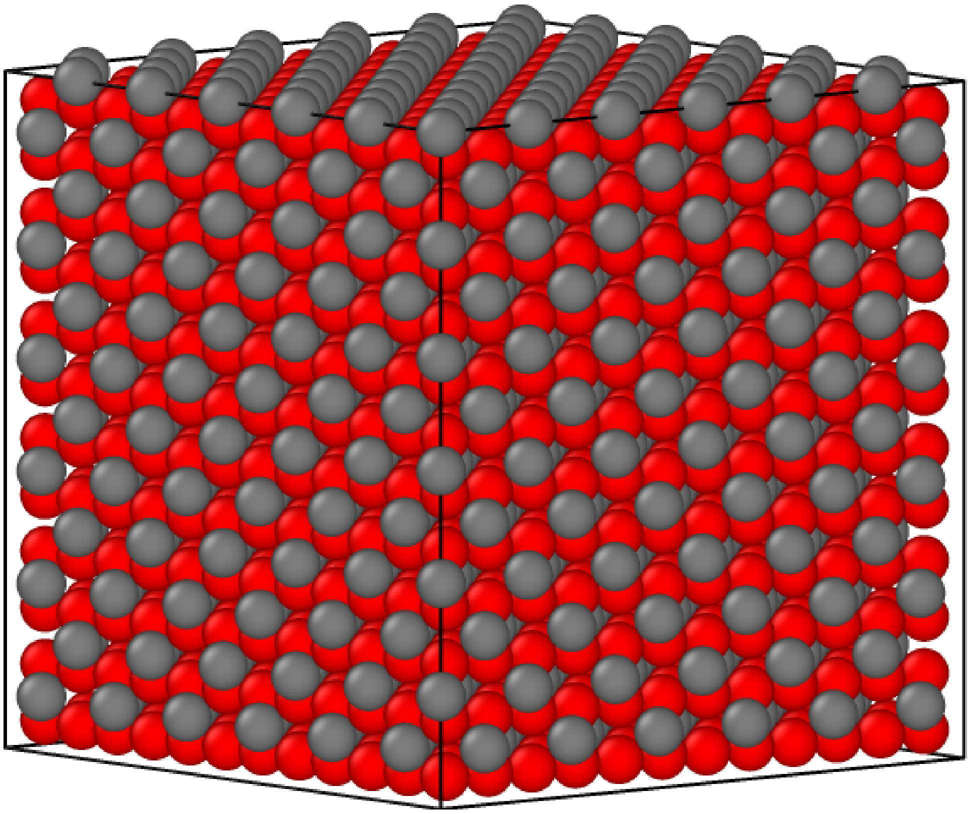

Figure S2: The $6 \times 6 \times 6$ supercell built in LAMMPS using the CIF. This is the initial configuration used in the relaxation simulations.

In order to optimize the initial box structure, a minimization/relaxation was carried out following the steps:

- Cojungated Gradient minimization simulation.
- NpT simulation at 300 K at 1 MPa for 100 ps.
- Steep Descent minimization simulation.
- Cojungated Gradient minimization simulation.
- NpT simulation at at 1500 K at 1 MPa for 100 ps.

In the above steps, all atoms were allowed to move and periodic boundary conditions (PBC) in the 3 dimensions was applied.

2.2 Nanoparticle Ammorphisation

After the crystal relaxation, we proceeded with the amorphisation. We started from the configuration containing the $6 \times 6 \times 6$ crystal relaxed structure and 15.0 Å of vacuum in all sides. Figure S3 shows the initial box structure used in the nanoparticle ammorphisation. The vacuum regions were added to avoid any contact between the particle and its images generated by the periodic boundary condition. Additionally, Lennard–Jones walls were set around the box in all the directions to avoid that the atoms move between the PBC boxes due to the high temperature used in the simulation. In LAMMPS, this approach is performed using `fix wall/lj126`. The ε and σ were $1.0\,\text{eV}\,\text{Å}^{-2}$ and 5.0 Å with a 5.0 Å cutoff. Those values were selected to ensure a higher repulsion in the walls in comparison to the NP internal forces.

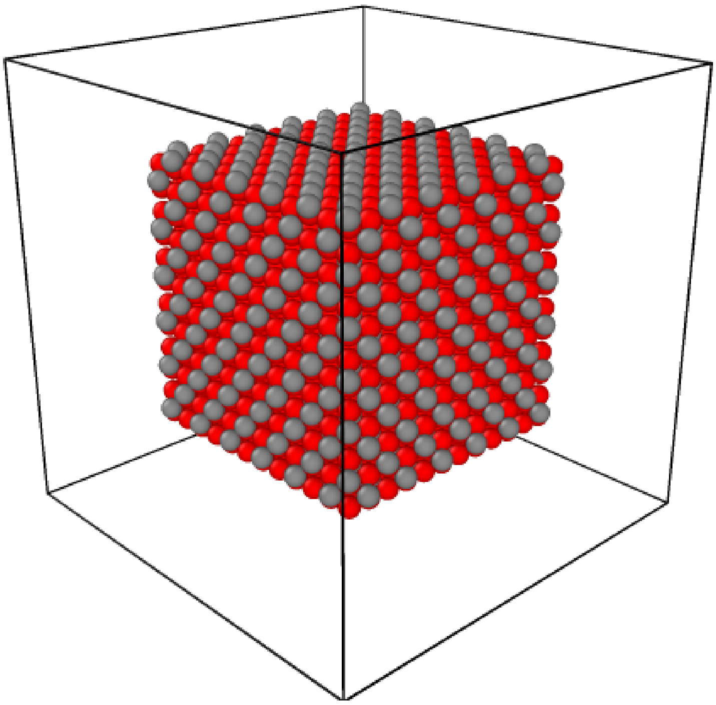

Figure S3: Simulation box containing the relaxed $6 \times 6 \times 6$ CeO_2 supercell and 15.0 Å of vacuum in all sides.

The role of the amorphisation is to generate a particle without any structural correlation with the initial structure simulation, Figure S3. The Sayle's group perform simulations in high temperatures applying constant forces to speedup the amorphisation step and ensure that all the initial structure was lost. In our work, the amorphisation can be summarized in the following stages:

1. NVT simulation at 4500 K for 200 ps, in which one 2 layers are flexible and 4 layers are kept fixed.
2. NVT simulation at 4500 K for 300 ps, in which one 4 layers are flexible and 2 layers are kept fixed.
3. NVT simulation at 4500 K for 100 ps, in which all particles and layers are allowed to move.
4. NVT simulation at 4500 K for 700 ps with tension applied in the crystal to improve the amorphisation.
5. Annealing NVT simulation from 4500 K to 5500 K for 400 ps.
6. NVT simulation at 5500 K for 100 ps.
7. 1000 ps NVT simulation with temperature ramp from 5500 K to 8500 K, in the end the CeO_2 amorphous sample is obtained.

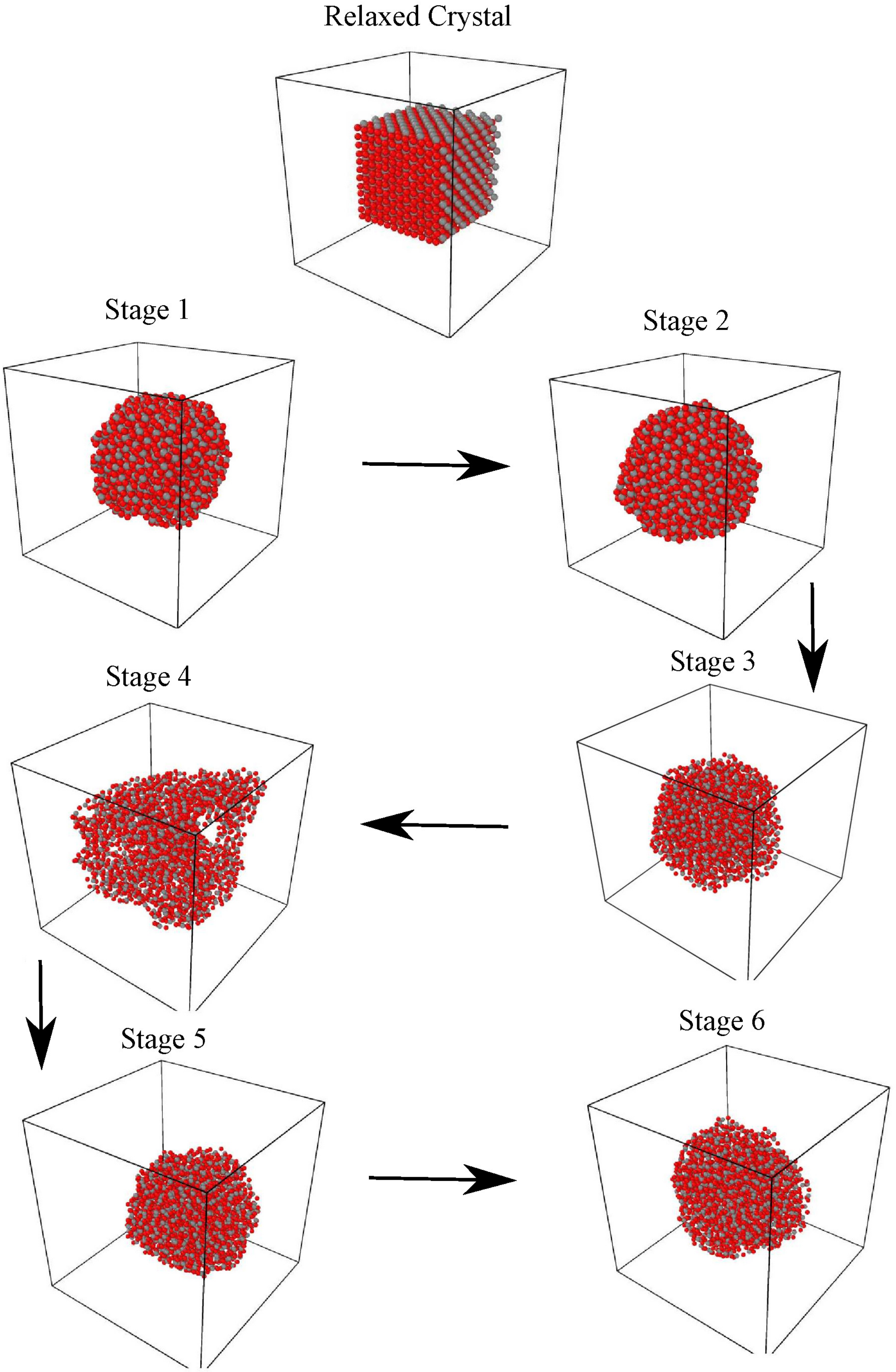

Figure S4: Last configuration of each amorphisation step described above. Last configuration at Stage 6 is the full amorphised CeO_2 nanoparticle.

Figure S4 shows the final configuration of each amorphisation stage in the nanoparticle amorphisation simulation. The nanoparticle configuration shown at the stage 6 is the fully amorphised CeO_2 nanoparticle.

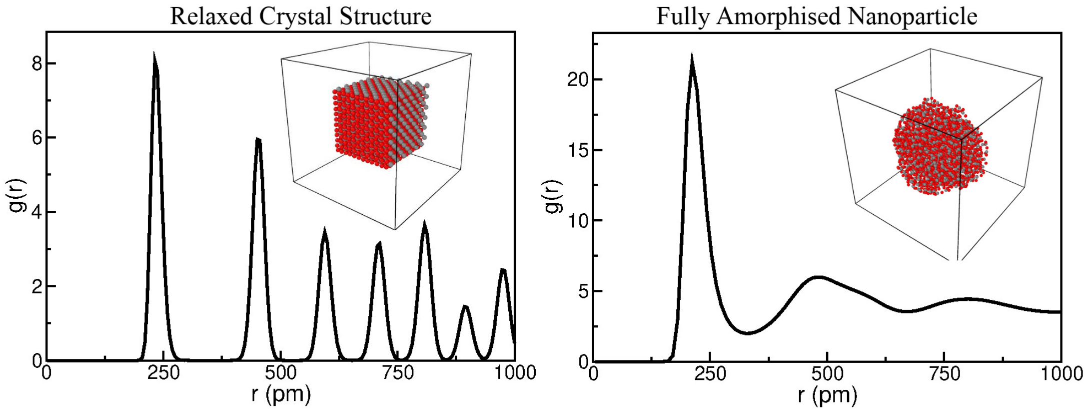

Figure S5: Radial distribution function for the Ce - O interaction in the relaxed crystal structure and the fully amorphised nanoparticle structure

Figure S4 show that the nanoparticle was fully amorphised and the cubic initial configuration was lost. However, to prove that all the initial structure was lost, radial distribution functions ($g(r)$) for the Ce - O interaction were calculated for the relaxed crystal structure and for the last configuration in the amorphisation simulation. Looking to the rdfs in Figure S5 is possible see that the well defined peaks in the relaxed crystal structure were lost and the fully amorphous structure has a "liquid-like" profile, with less defined peaks. Therefore, we can conclude that the CeO_2 nanoparticle has a entire different structure from the crystal.

3 Recrystalization Tests

Once the amorphisation process defined, several recrystalization protocol were tested to find the best one to generate the CeO_2 nanoparticle. Two main approaches were defined, (i) the annealing decreasing the temperature from 5500 K until reach 0.0 K in alternated temperature ramps and fix temperature equilibrations, and (ii) the annealing also from from 5500 K to 0.0 K, but done in a single temperature ramp.

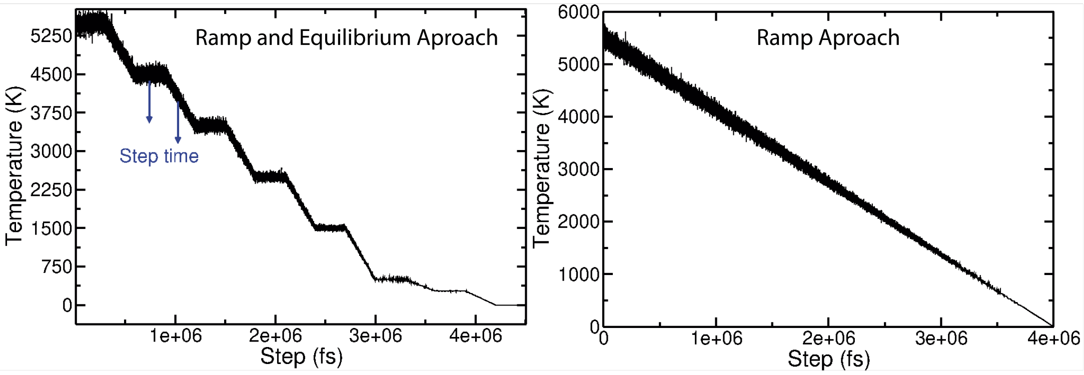

Figure S6: Recrystalization approaches. At right, we show the Ramp and Equilibrium Steps approach, the temperature is decreased in small ramps and consequent short equilibrium stages. Several tests were performed with different ΔT and step times. At Left, the Ramp approach. Decreasing of the temperature from 5500 K directly to 0 K. The simulation time and consequently the temperature rate can be changed.

Several temperature rates and total simulation times were tested in both recrystalization approaches described above. The following tests were carried out:

1. Ramp and equilibrium steps, 50 ps each step and ΔT 1000 K - Trajectory length 850 ps - **D1000-50**
2. Ramp and equilibrium steps, 100 ps each step and ΔT 1000 K - Trajectory length 1700 ps - **D1000-100**
3. Ramp and equilibrium steps, 200 ps each step and ΔT 1000 K - Trajectory length 3400 ps - **D1000-200**
4. Ramp and equilibrium steps, 300 ps each step and ΔT 1000 K - Trajectory length 5100 ps - **D1000-300**
5. Ramp and equilibrium steps, 50 ps each step and ΔT 100 K - Trajectory length 5050 ps - **D100-50**
6. Ramp and equilibrium steps, 100 ps each step and ΔT 100 K - Trajectory length 10 100 ps - **D100-100**
7. Ramp and equilibrium steps, 200 ps each step and ΔT 100 K - Trajectory length 20 200 ps - **D100-200**

8. Ramp and equilibrium steps, 300 ps each step and ΔT 100 K - Trajectory length 30 300 ps - **D100-300**

9. Ramp and equilibrium steps, 500 ps each step and ΔT 100 K - Trajectory length 51 000 ps - **D100-500**

10. Ramp and equilibrium steps, 1000 ps each step and ΔT 100 K - Trajectory length 51 000 ps - **D100-1000**

11. Ramp, fix temperature rate 2.750 $\mathrm{K\,ps^{-1}}$ - Trajectory length 2000 ps - **R2**

12. Ramp, fix temperature rate 1.375 $\mathrm{K\,ps^{-1}}$ - Trajectory length 4000 ps - **R4**

13. Ramp, fix temperature rate 0.917 $\mathrm{K\,ps^{-1}}$ - Trajectory length 6000 ps - **R6**

14. Ramp, fix temperature rate 0.550 $\mathrm{K\,ps^{-1}}$ - Trajectory length 10 000 ps - **R10**

15. Ramp, fix temperature rate 0.275 $\mathrm{K\,ps^{-1}}$ - Trajectory length 20 000 ps - **R20**

16. Ramp, fix temperature rate 0.1375 $\mathrm{K\,ps^{-1}}$ - Trajectory length 40 000 ps - **R40**

17. Ramp, fix temperature rate 0.055 $\mathrm{K\,ps^{-1}}$ - Trajectory length 100 000 ps - **R100**

Figure S7 shows the last configuration of each annealing approach explained above.

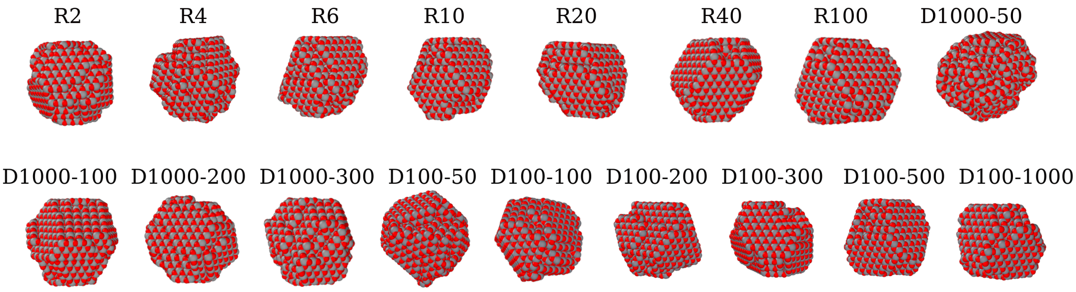

Figure S7: Last frame of the CeO_2 structures generated by all the annealing simulations carried in the tests step. The caption above the structure means the name of the annealing approach used to generate it.

Once the annealing simulations have reached the 0 K, 2000 ps production simulations at 0 K were performed to generate data for the calculation of the structural and energetic properties of interest. Figures S8, S9 and S10 are the total potential energies, volume and surface areas of the CeO_2 nanoparticles at 0 K obtained with OVITO.

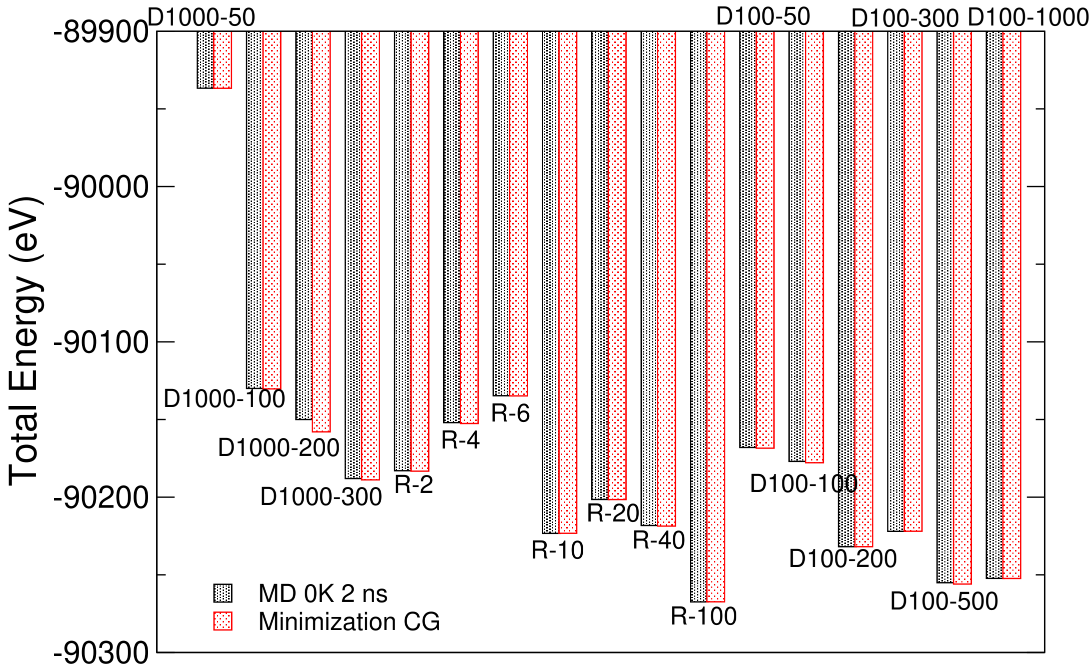

Figure S8: Total potential energies for the CeO_2 nanoparticles. The gray columns are the total energies for 2.0 ns of simulation at 0.0 K, while the red columns are the total energies for the minimized CeO_2 nanoparticle. The minimization were performed for the last configurations from the 2.0 ns simulation, to ensure that the nanoparticles were in the minimum energy.

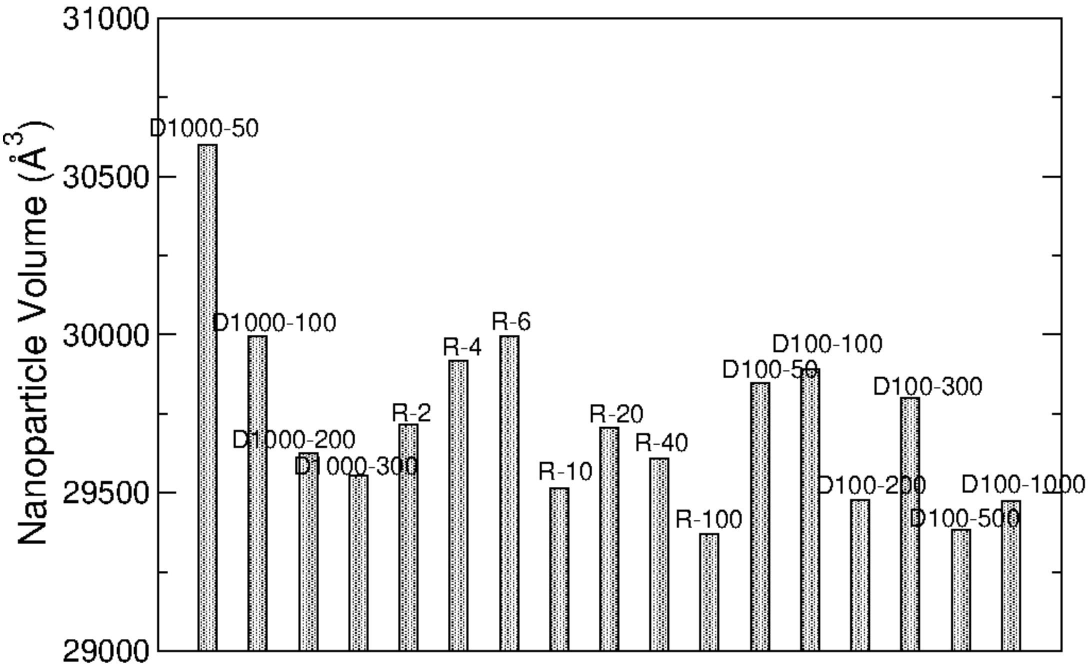

Figure S9: Nanoparticles volumes for the CeO_2 nanoparticles at 0 K.

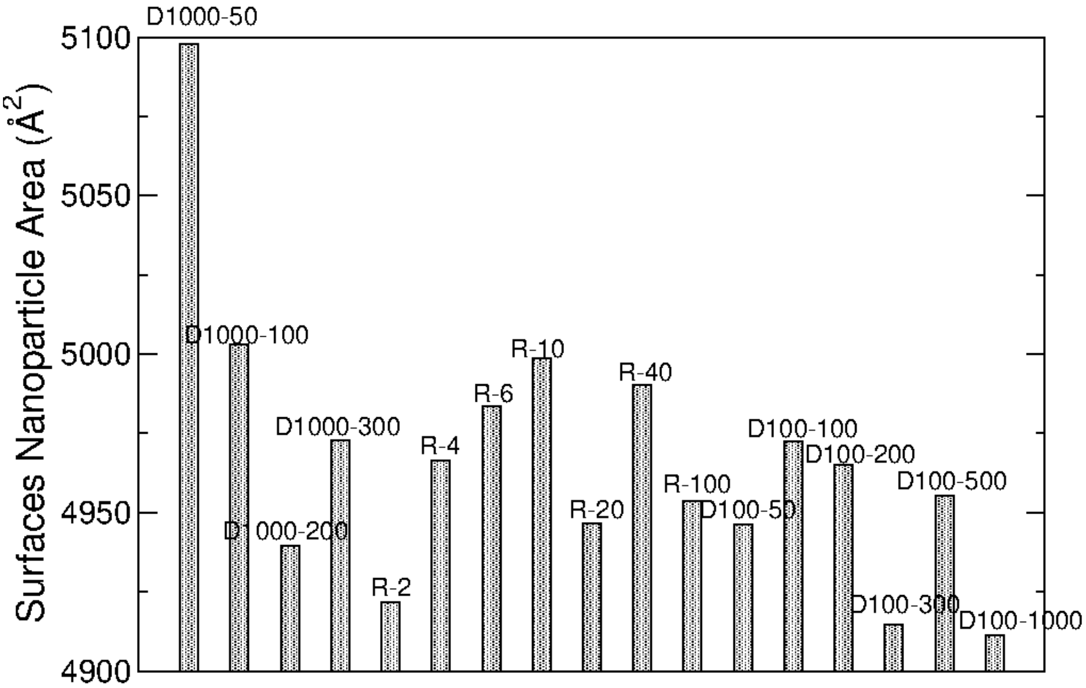

Figure S10: Surface area for the CeO_2 nanoparticles at 0 K. For the Nanoparticles names, check above.

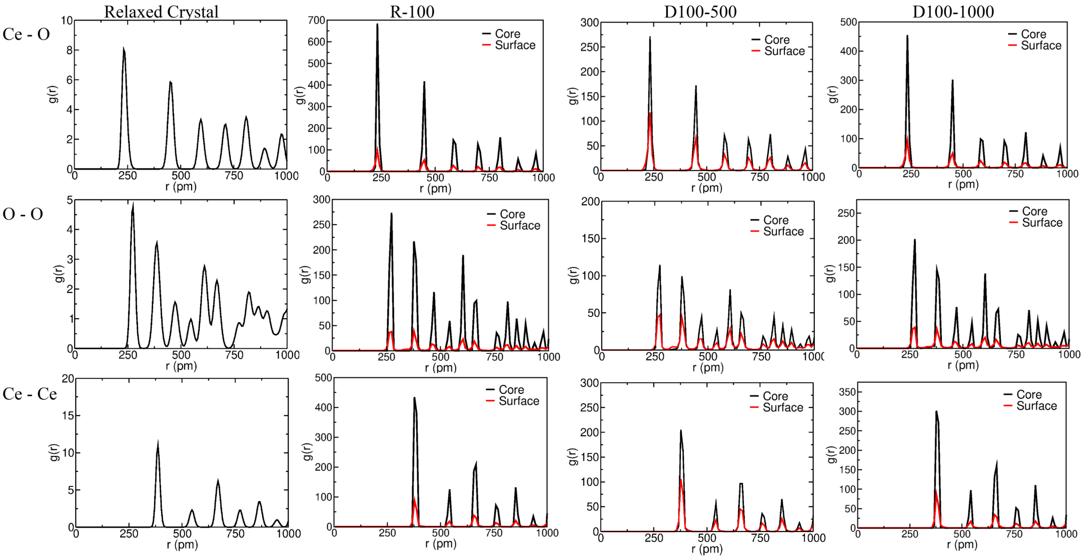

Figure S11: Radial distribution functions ($g(r)$) for the pairs Ce – O, O – O and Ce – Ce in the surface and core regions for the lowest energy nanoparticles from the annealing tests (R-100, D100-500 and D100-1000, Figure S7), as well as the relaxed crystal structure, Figure S3. Only very small differences can be seen in the plots for the annealed particles, showing that they display the same local ordering.

4 Final Recrystallization Protocol Details

In virtue of recent literature contributions of Sayle group,[6,7] we are using for the recrystallization process the potential parameters as the ones used by Grimes group.[8] The new parameters set (see table on main paper) was tested and directly compared with the original parameters set to certify that we can choose the best parameters to represent the physical nature of this system. We have run a series of simulations with Sayle's parameter set. We did not performed the full analysis on those test calculation, but we performed XRD and vacancy characterizations, because they open the opportunity of direct comparing results to experimental measurements. Figures S13 and S14 present sample analysis with the structures obtained using original Sayle's potential parameters.

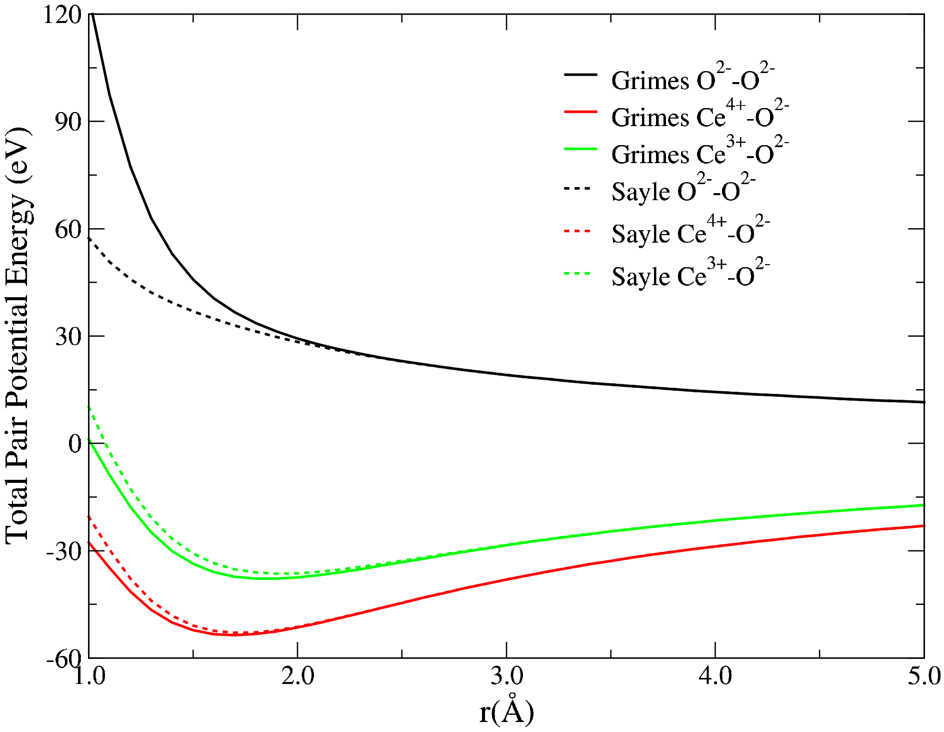

Figure S12: Comparison between Sayle and Grimes proposed pair potential, including Buckingham and Coulomb interaction, for CeO_2 and Ce_2O_3.

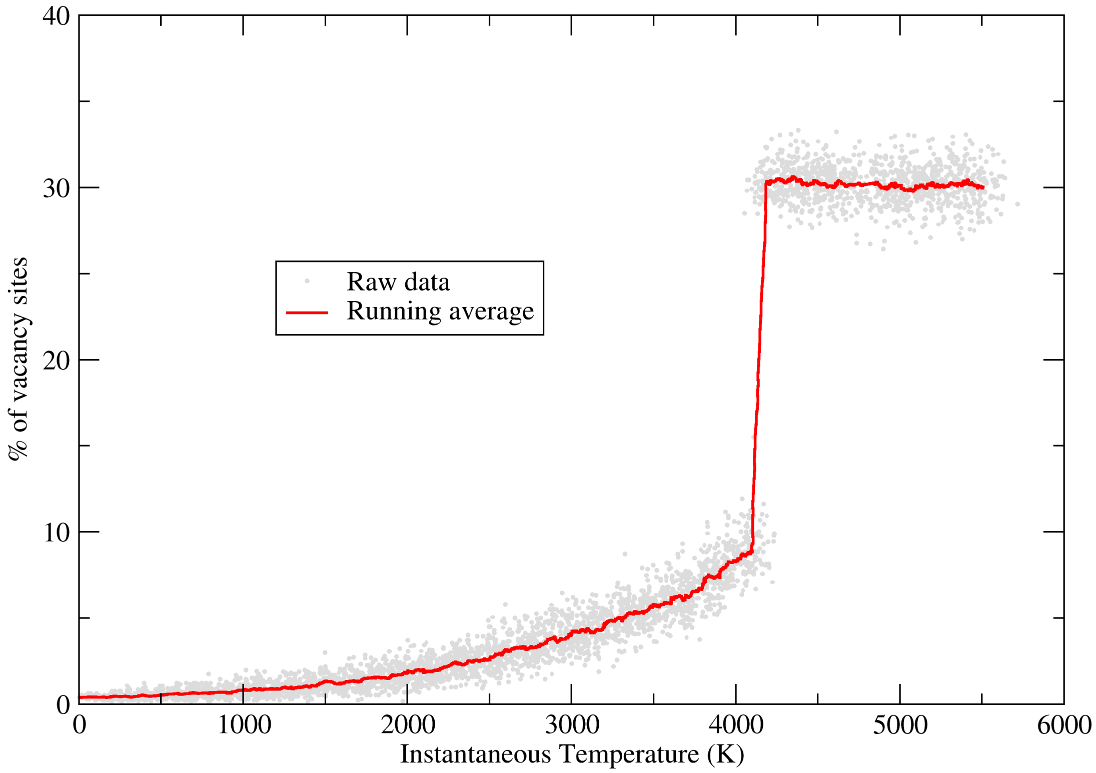

Figure S13: Sample of the analysis regarding number of vacancies in a structure as function of the temperature in the annealing process. This result was obtained for a 6 × 6 × 6 CeO_2 nanoparticle.

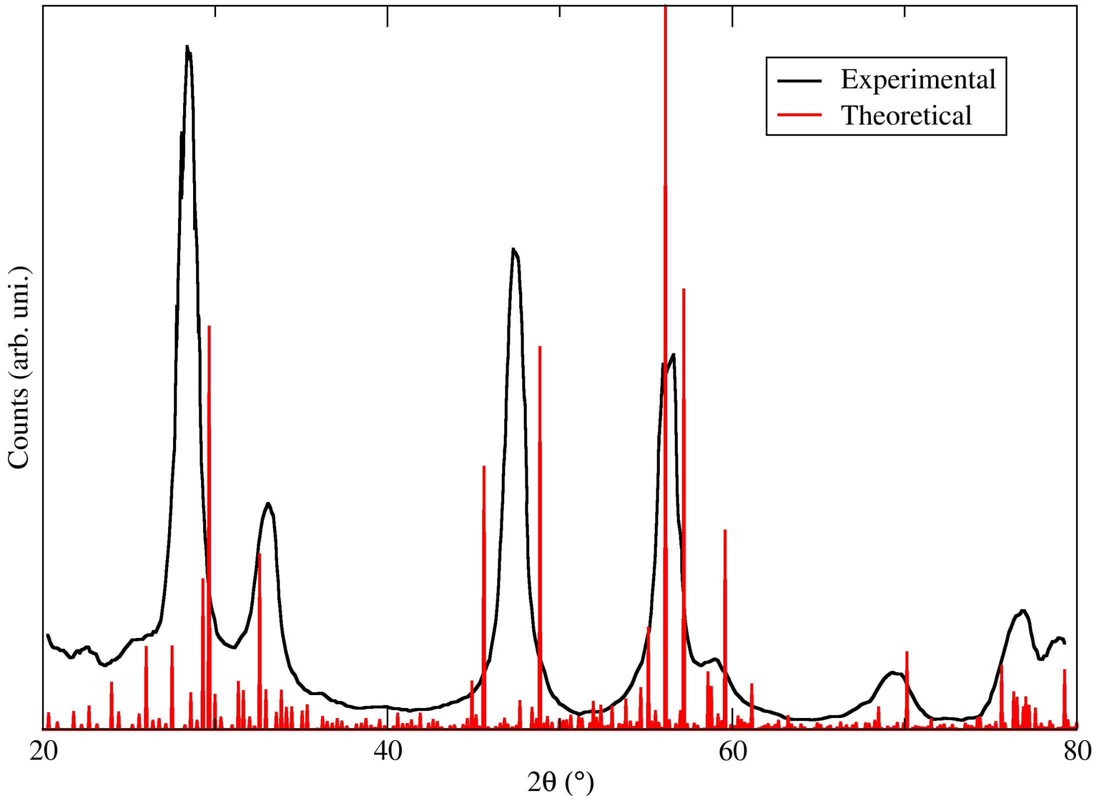

Figure S14: Sample of the XRD calculated by LAMMPS for our 6 × 6 × 6 CeO_2 nanoparticle at 300 K (non-equilibrium single frame). The experimantal result was extracted from reference[9].

5 Umbrella Sampling Details

In special cases where the system can be described as a reaction coordinate R, the biased free energy $F_{\text{Biased}}(R)$ can be written as the sum of the unbiased free energy $F_{\text{Unbiased}}(R)$ with the $\Omega_n(R)$ function,[10,11]

$$\Omega_n(R) = \frac{1}{2}K(R - R_0)^2 \ , \tag{1}$$

where Ω_n is a harmonic potential, K is the force constant and n the MD window in which the US is calculated. The unbiased free energy is obtained from the thermodynamic average of the distribution function described below,

$$\Phi(R) = \frac{\int \delta(R_r - R) e^{\frac{-E(\mathbf{r}^N)}{k_B T}} d\mathbf{r}'^N}{\int e^{\frac{-E(\mathbf{r}^N)}{k_B T}} d\mathbf{r}'^N} \ , \tag{2}$$

where $\Phi(R)$ represents the probability distribution in all simulation frames and $E(\mathbf{r}^N)$ is the potential energy. In this way, unbiased free energy is obtained using the US technique using the following equation,

$$F_{\text{Unbiased}}(R) = \frac{1}{k_B T} ln(\Phi(R)) - \Omega_n(R) + F_m \ . \tag{3}$$

The constant F_m arises naturally due to the self-consistent nature of the method, by minimizing the displacement of free energy between different MD frames. In this way, applying US simulations in series, we can obtain the energy barrier between two regions of the simulated model. Weighted average free energies are obtained using the weighted histogram analysis method (WHAM),[12] which evaluates a weighted average of the individual window distributions generated by MD simulations.

6 Additional Data for $6 \times 6 \times 6$ Supercell Particle

6.1 Density versus Temperature plot

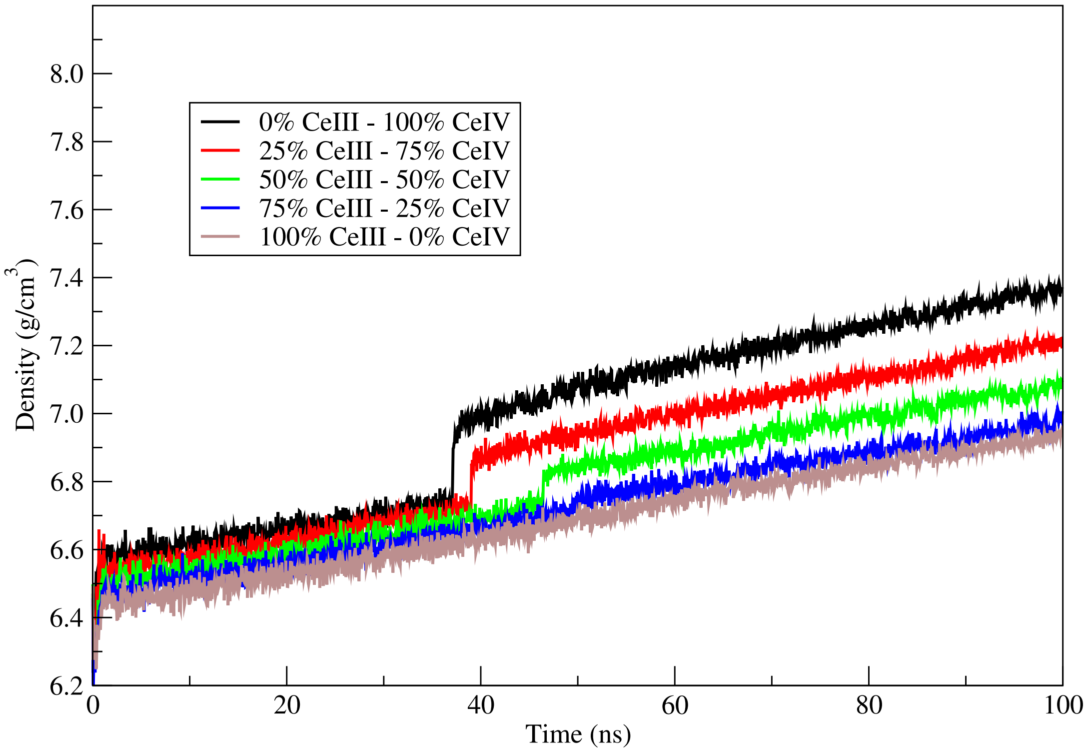

Figure S15: Density evolution in the system as time evolves in the annealing process. The results shown in this plot are from the $6 \times 6 \times 6$ CeO_2-Ce_2O_3 nanoparticles.

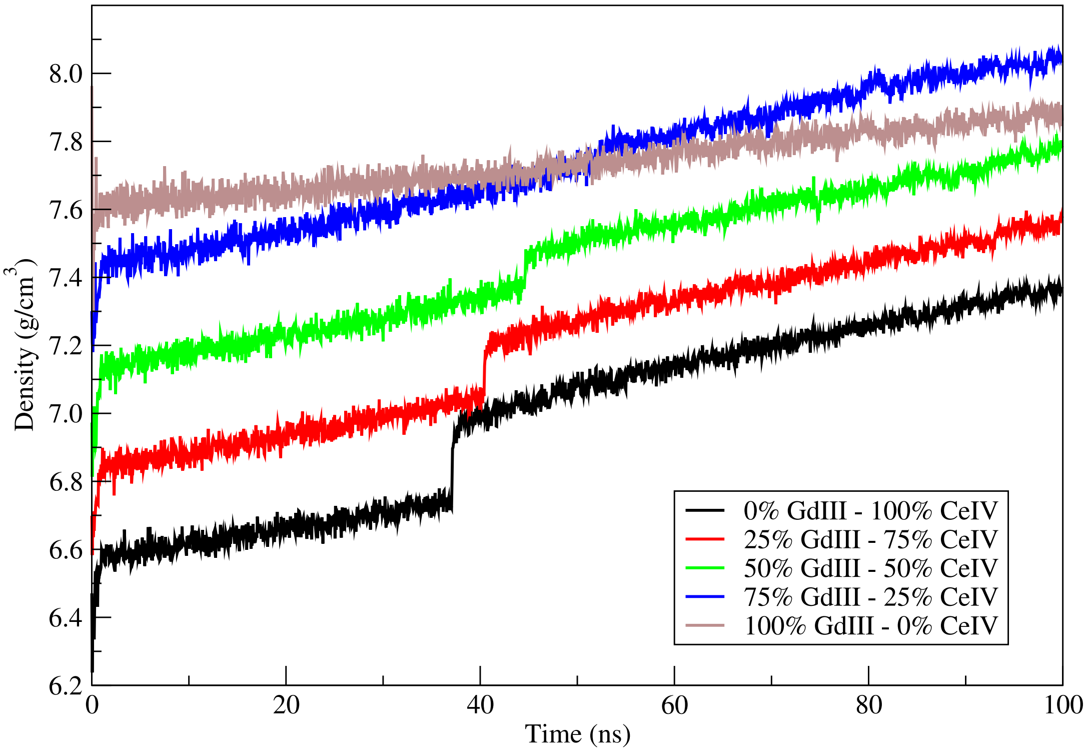

Figure S16: Density evolution in the system as time evolves in the annealing process. The results shown in this plot are from the 6 × 6 × 6 CeO_2-Gd_2O_3 nanoparticles.

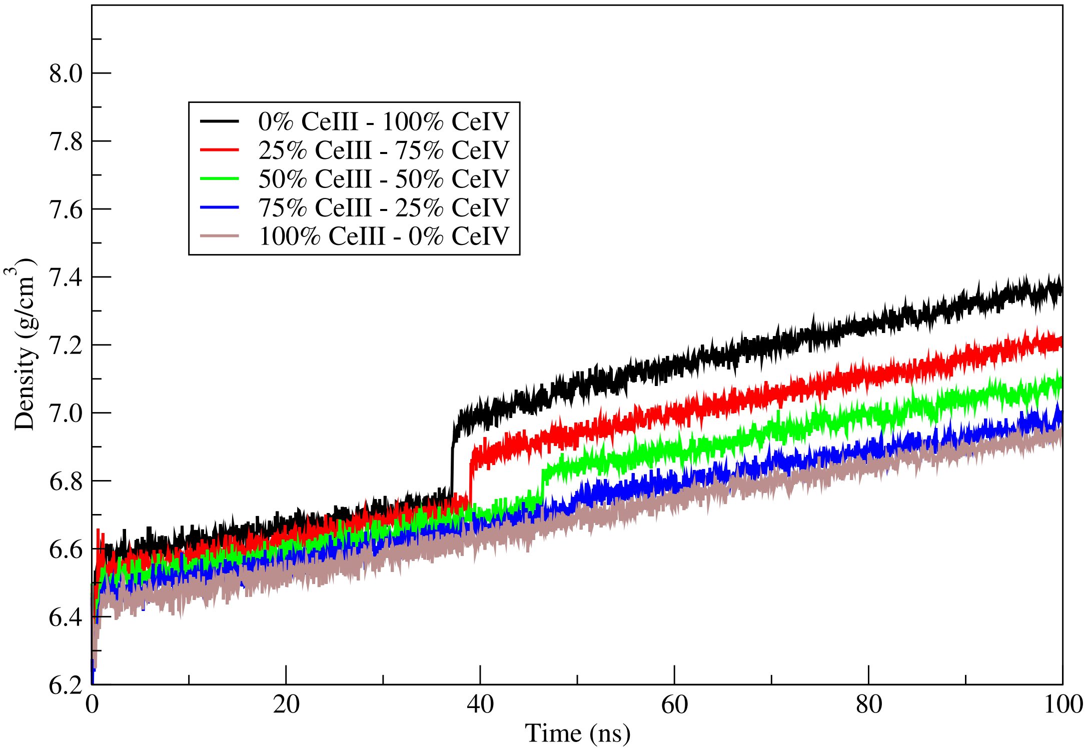

Figure S17: Density evolution in the system as time evolves in the annealing process. The results shown in this plot are from the 6 × 6 × 6 CeO_2-La_2O_3 nanoparticles.

6.2 XRD for pristine systems in all phases available in Material Project

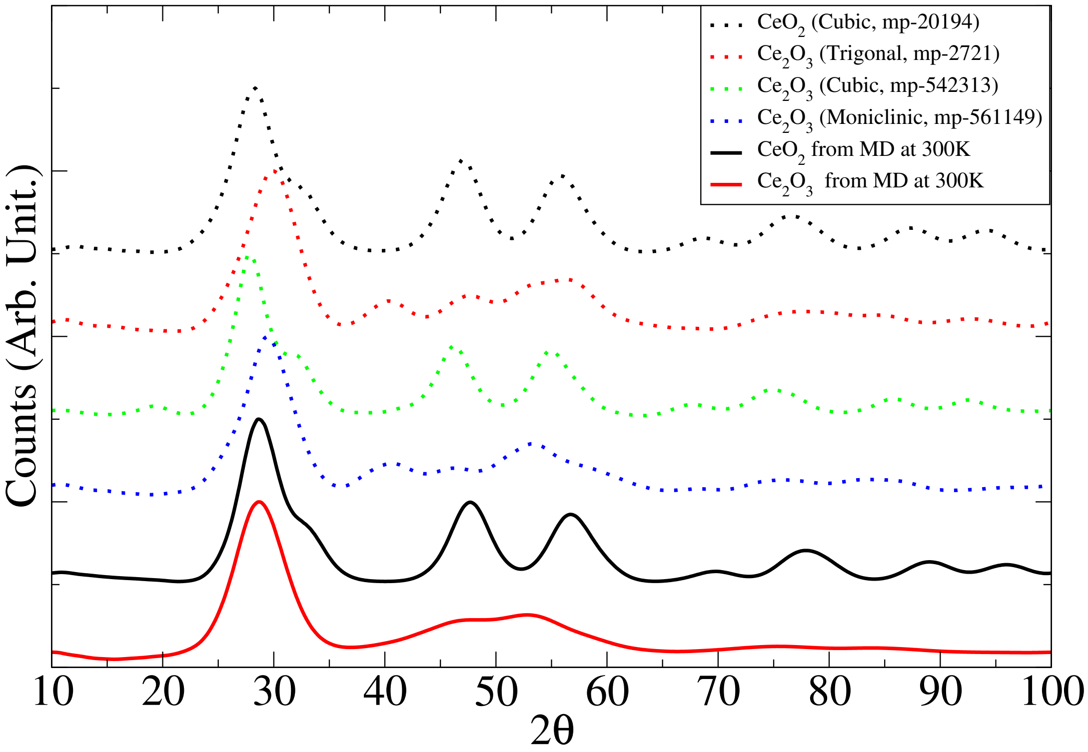

Figure S18: X-ray diffraction pattern obtained for our final structures for CeO_2 and Ce_2O_3 compered with the same materials from Materials Projects. For our results, we done a 300 K molecular dynamics using the 0 K structure, taking average XRD over 500 ps. For the structures from Materials Project, we build a $6 \times 6 \times 6$ supercell and done single frame XRD pattern. All data was post processed with an 1 / low-pass filter to remove noise.

6.3 $g(r)$ for all 0 K structures

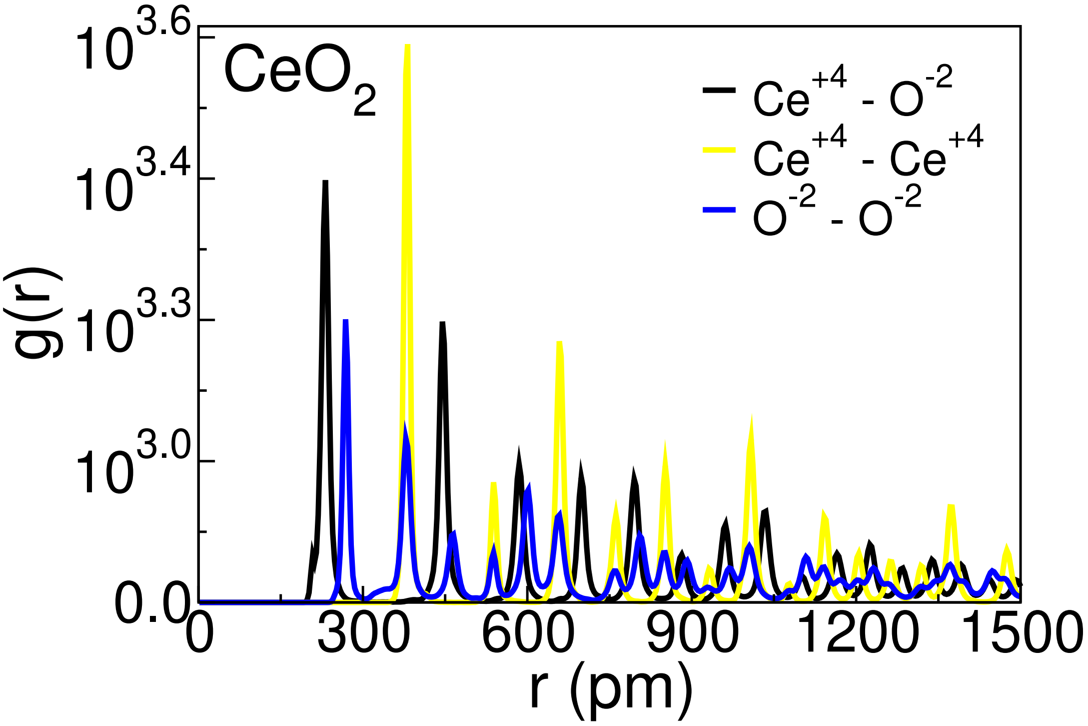

Figure S19: Partial $g(r)$ obtained for each pair or species in our final CeO$_2$ structure. This result is the average data from the same 500 ps 300 K molecular dynamic used to get XRD data.

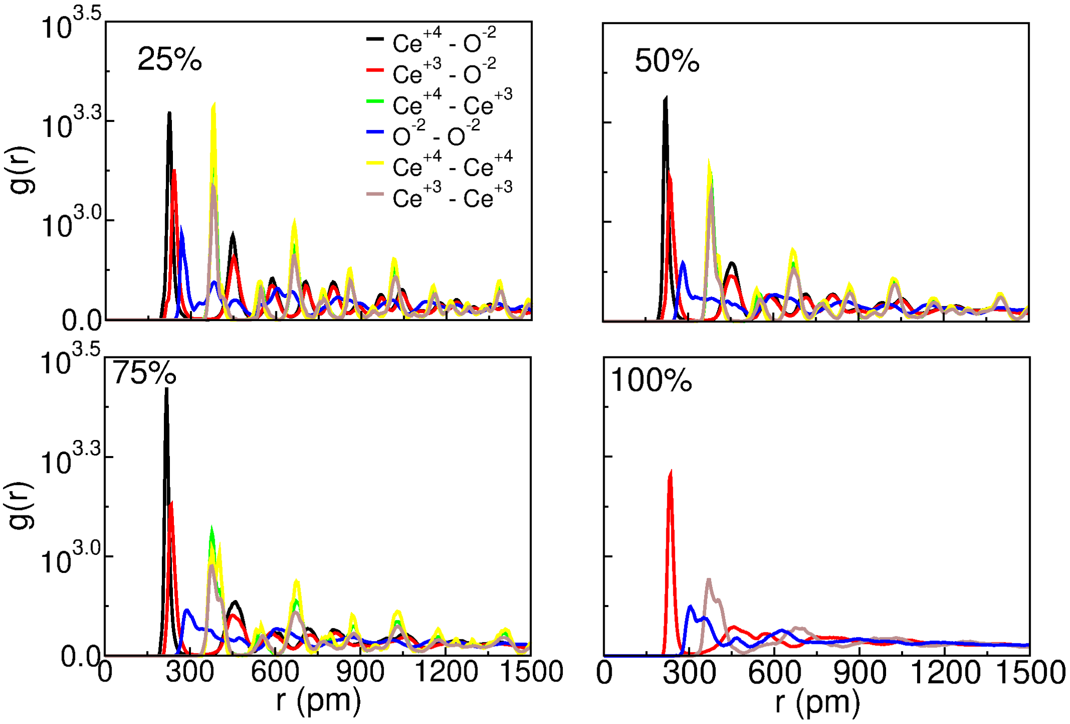

Figure S20: Partial $g(r)$ obtained for each pair or species in our final Ce^{3+} mixed structures. This result is the average data from the same 500 ps 300 K molecular dynamics used to get XRD data.

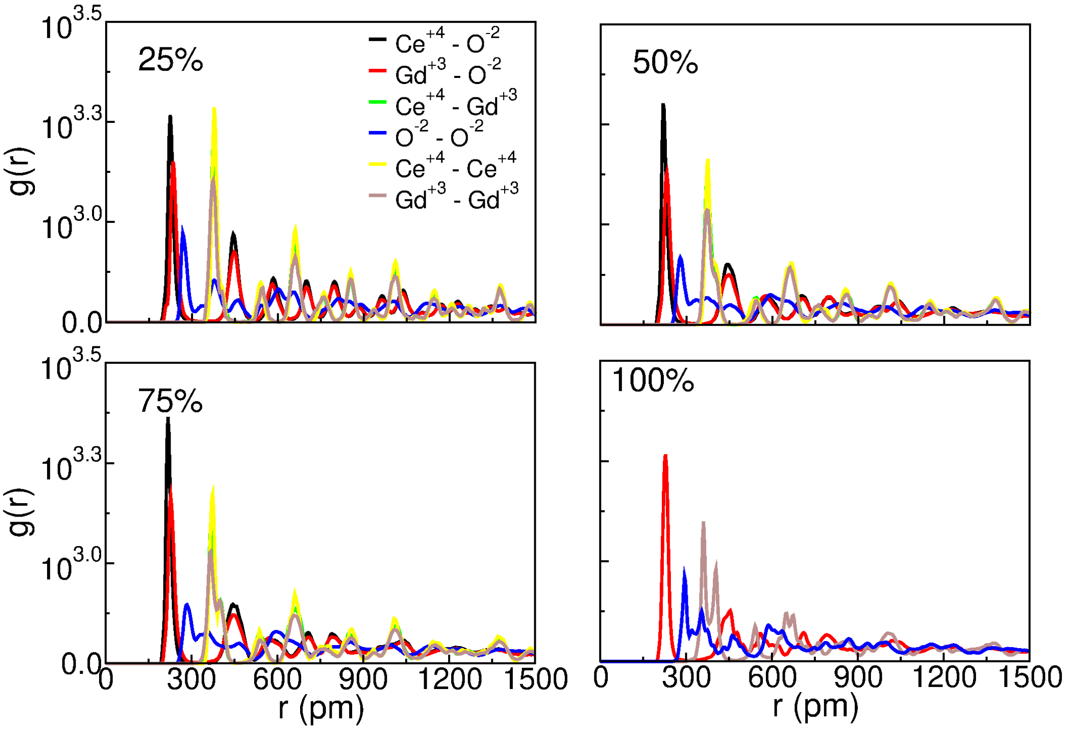

Figure S21: Partial $g(r)$ obtained for each pair or species in our final Gd^{3+} mixed structures. This result is the average data from the same 500 ps 300 K molecular dynamics used to get XRD data.

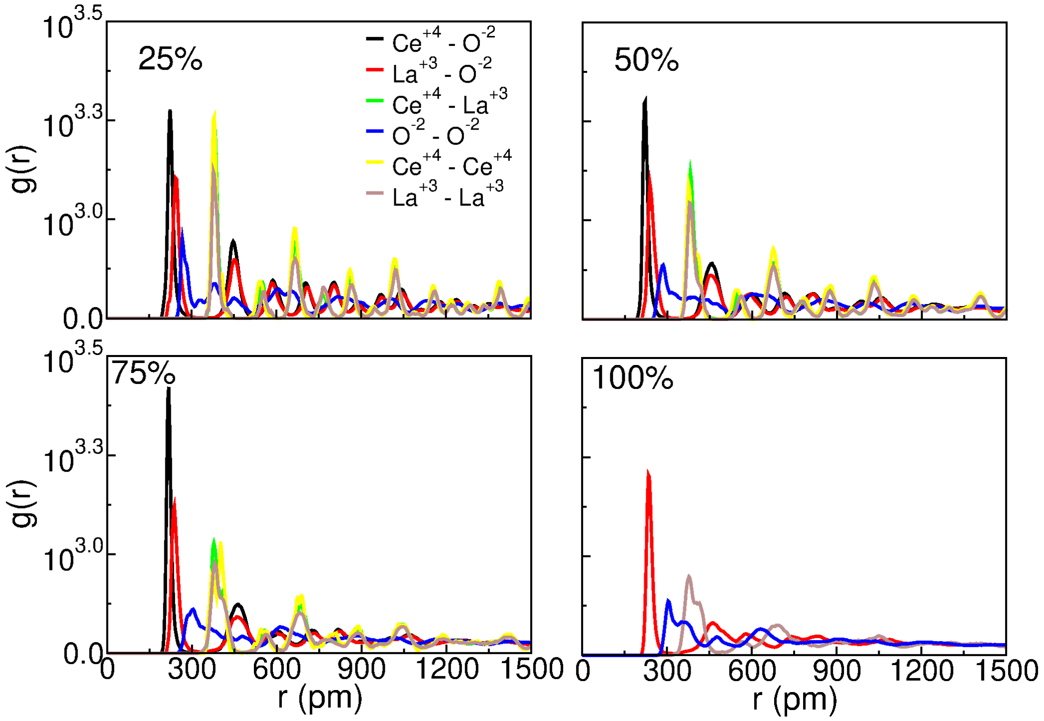

Figure S22: Partial $g(r)$ obtained for each pair or species in our final La^{3+} mixed structures. This result is the average data from the same 500 ps 300 K molecular dynamics used to get XRD data.

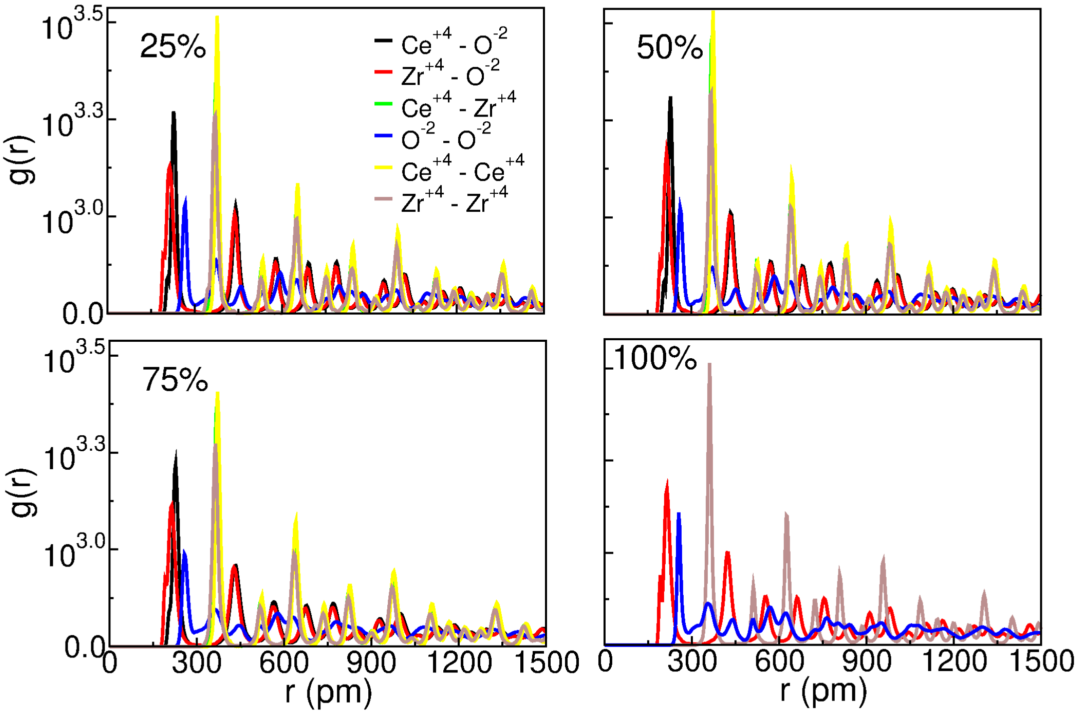

Figure S23: Partial $g(r)$ obtained for each pair or species in our final Zr^{4+} mixed structures. This result is the average data from the same 500 ps 300 K molecular dynamics used to get XRD data.

6.4 Radial Distribution Function at 0K

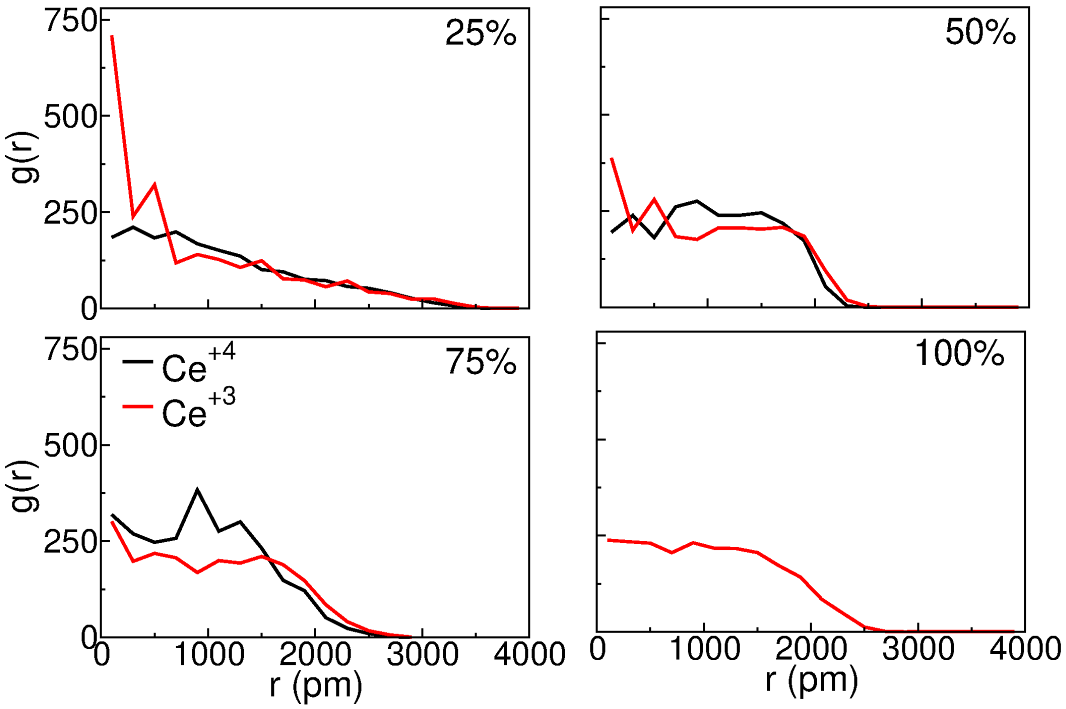

Figure S24: Radial distribution of cation species for the $6 \times 6 \times 6$ CeO_2-Ce_2O_3 mixed nanoparticles at 0 K.

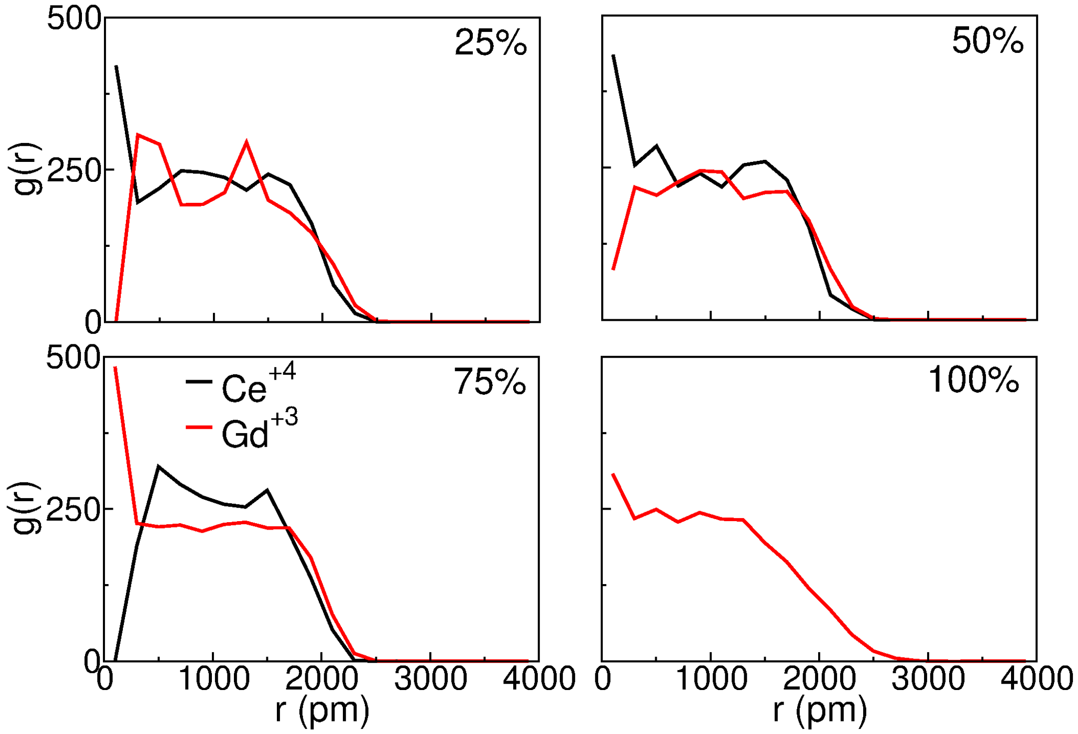

Figure S25: Radial distribution of cation species for the $6 \times 6 \times 6$ CeO_2-Gd_2O_3 mixed nanoparticles at 0 K.

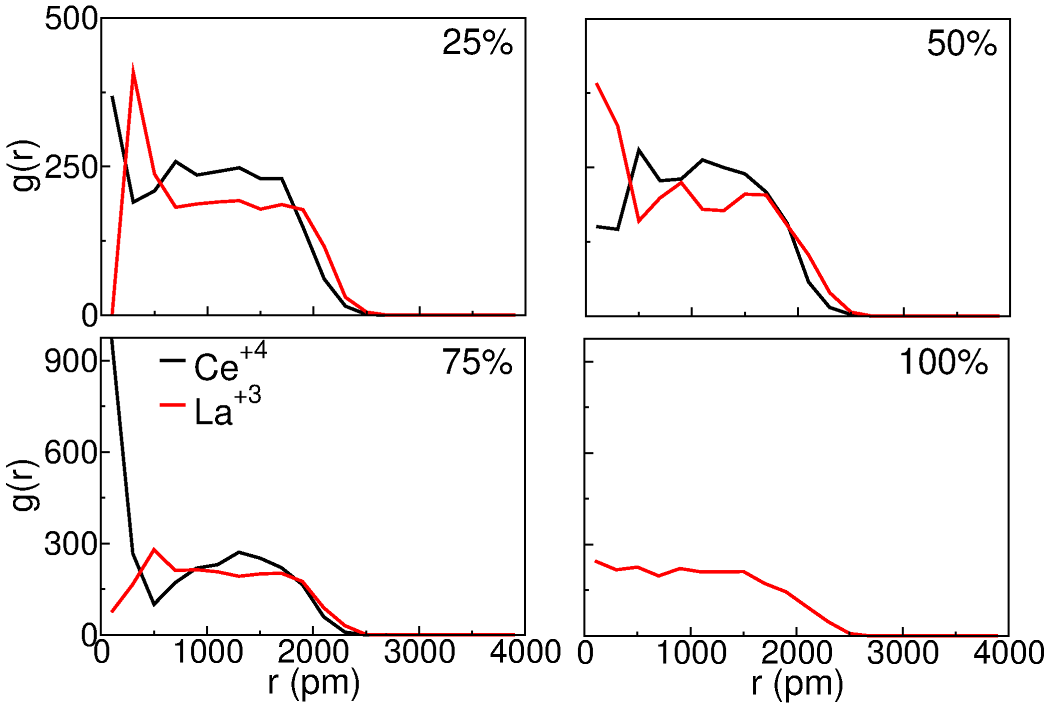

Figure S26: Radial distribution of cation species for the 6 × 6 × 6 CeO_2-La_2O_3 mixed nanoparticles at 0 K.

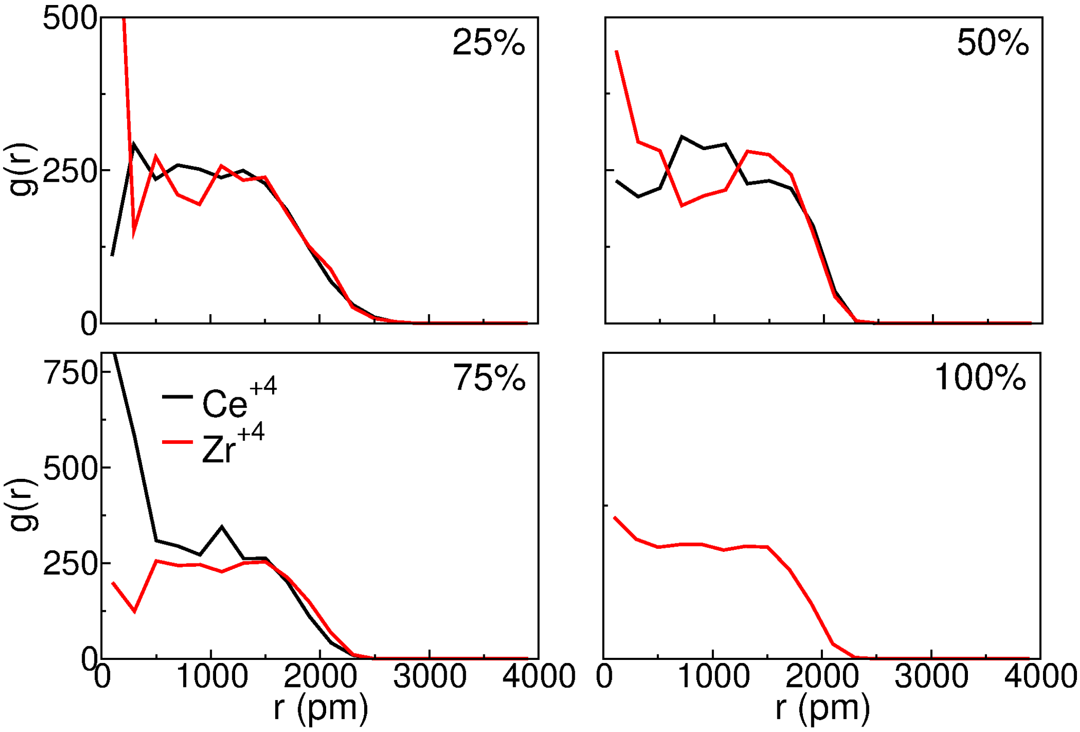

Figure S27: Radial distribution of cation species for the 6 × 6 × 6 CeO_2-ZrO_2 mixed nanoparticles at 0 K.

In a mixed system AB with radial distribution of particles of the specie A in relation to the geometric center described by the function $g_A(r)$, we can define:

$$g_{rel}^{A}(r) = \frac{g_A(r)}{g_A(r) + g_B(r) + \varepsilon} \tag{4}$$

where $epsilon = 0.001$ is included to prevent zero denominator error in the automated obtaining of this data. The physical meaning of $g_{rel}^{A}(r)$ is that it you chose randomly a particle P particle (that can be only one of the species A and B) that is r_P apart from the geometric center of the system, the probability that this particle is of the type A is given by $g_{rel}^{A}(r_P)$.

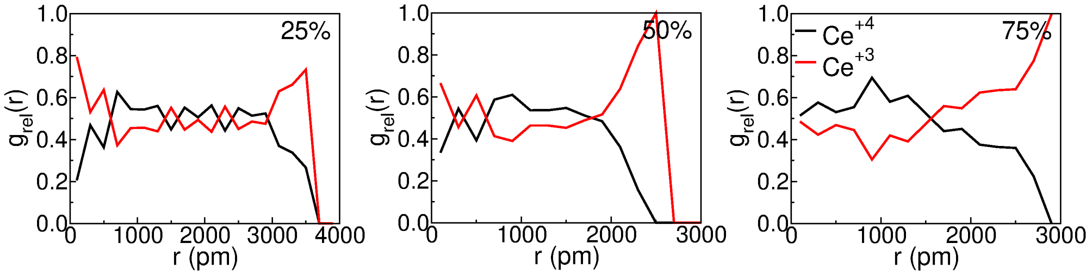

Figure S28: Relative radial distribution of cation species for the $6 \times 6 \times 6$ CeO_2-Ce_2O_3 mixed nanoparticles at 0 K.

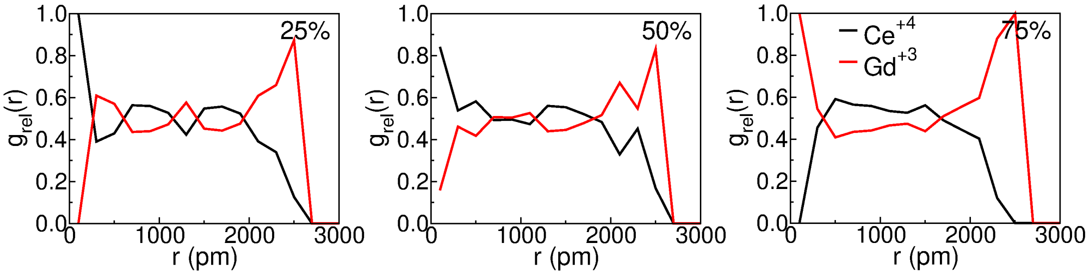

Figure S29: Relative radial distribution of cation species for the $6 \times 6 \times 6$ CeO_2-Gd_2O_3 mixed nanoparticles at 0 K.

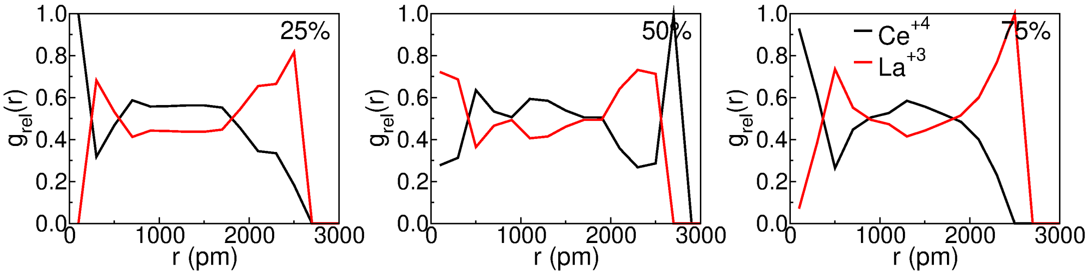

Figure S30: Relative radial distribution of cation species for the $6 \times 6 \times 6$ CeO_2-La_2O_3 mixed nanoparticles at 0 K.

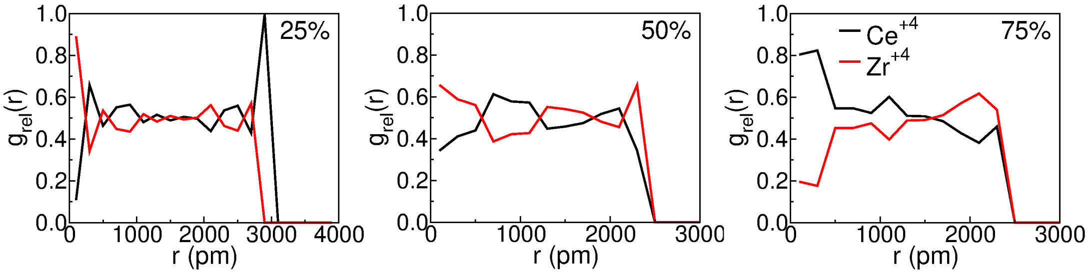

Figure S31: Relative radial distribution of cation species for the 6 × 6 × 6 CeO_2-ZrO_2 mixed nanoparticles at 0 K.

6.5 Excess Energy plot for each alloying specie

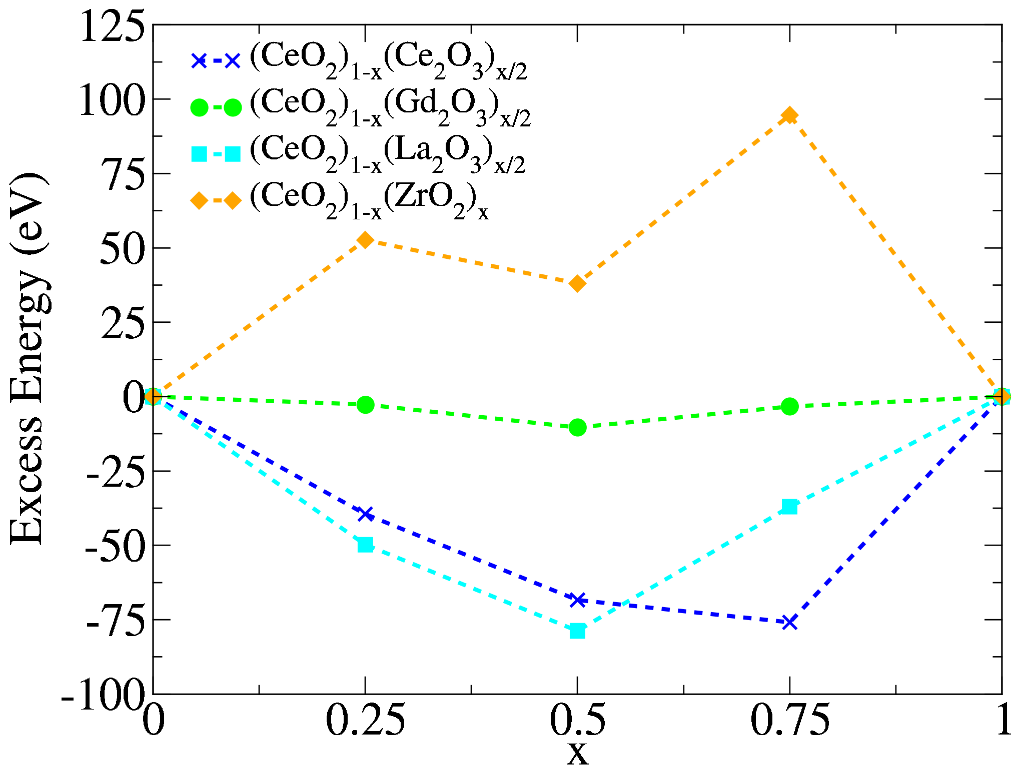

Figure S32: Excess energy plot for the obtained systems as used in x-ray diffraction (300 K).

6.6 Vacancy Creation Energy in pure CeO_2

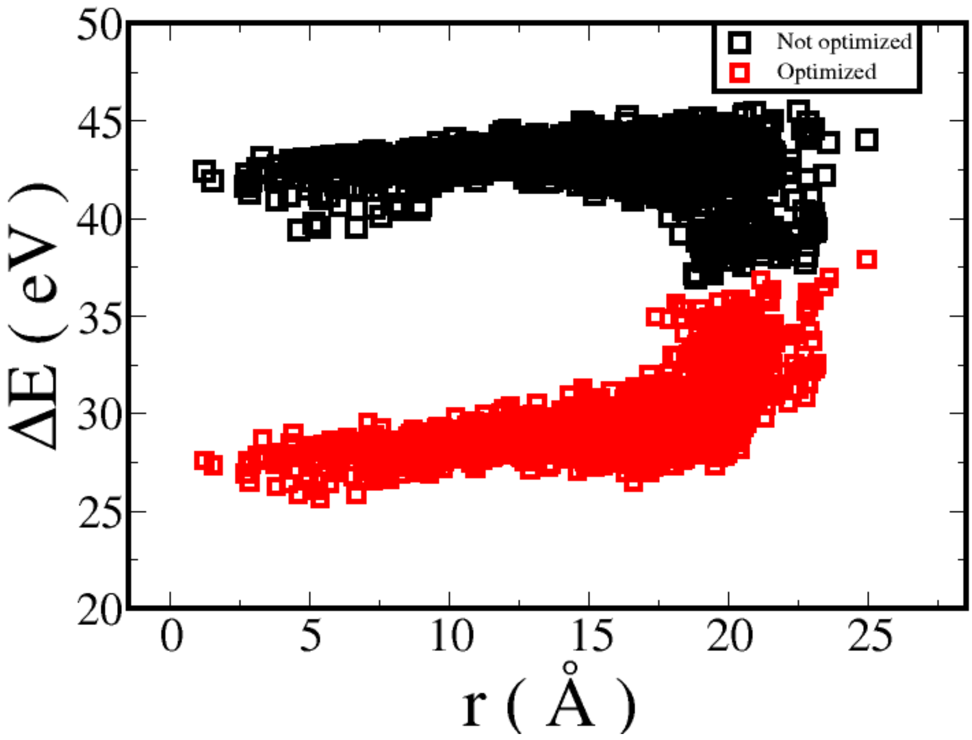

Figure S33: Variation of energy in the creation of vacancies as a function of the nanoparticle radius. In red, vacancies in the optimized structure have less energy variation than the not optimized structure in black.

6.7 Oxygen sites population

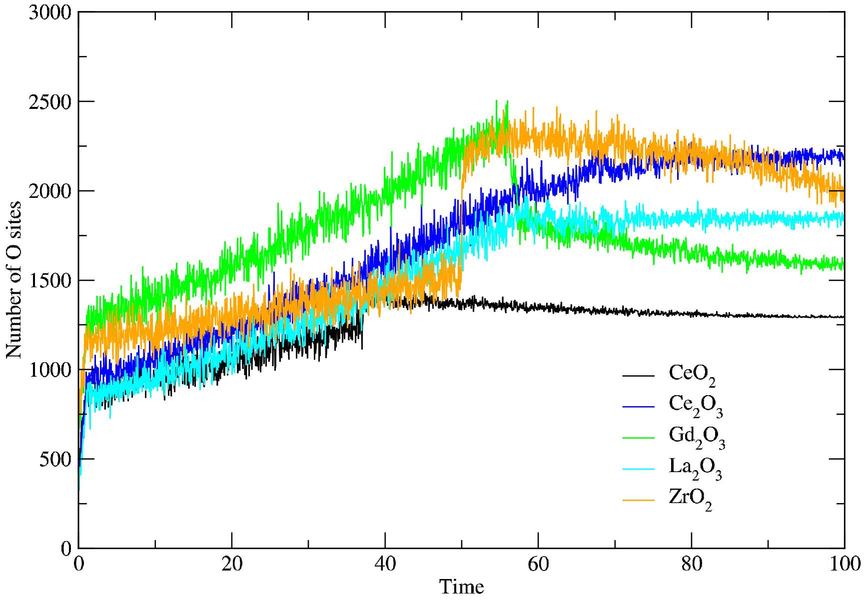

Figure S34: Evolution of the number of oxygen sites (or cation tetrahedra) in the pure systems.

7 Data for $5 \times 5 \times 5$ Supercell Particle

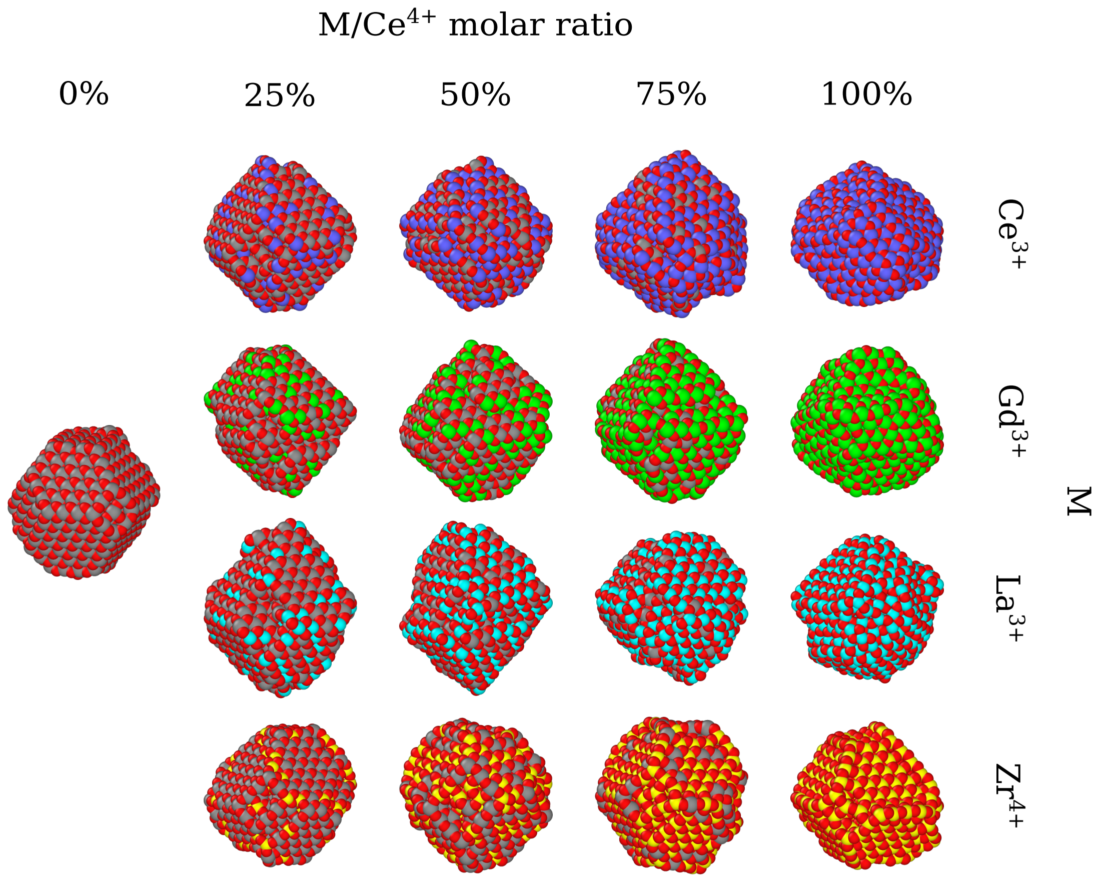

Figure S35: Final geometry, at 0 K, for the test cases starting from a $5 \times 5 \times 5$ supercell.

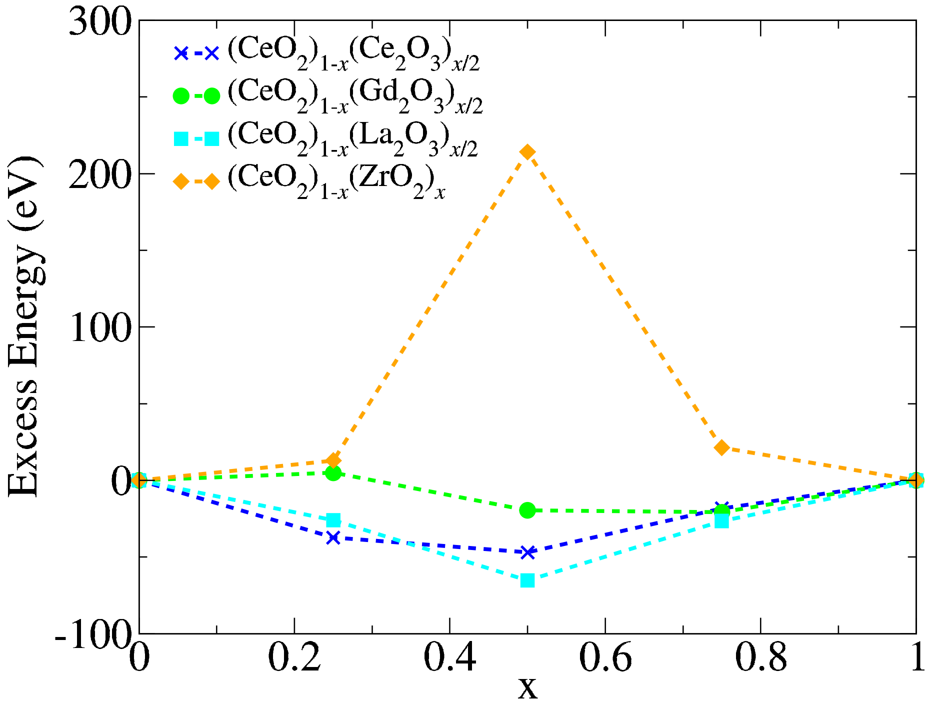

Figure S36: Excess energy calculated for the systems shown in Figure S35.

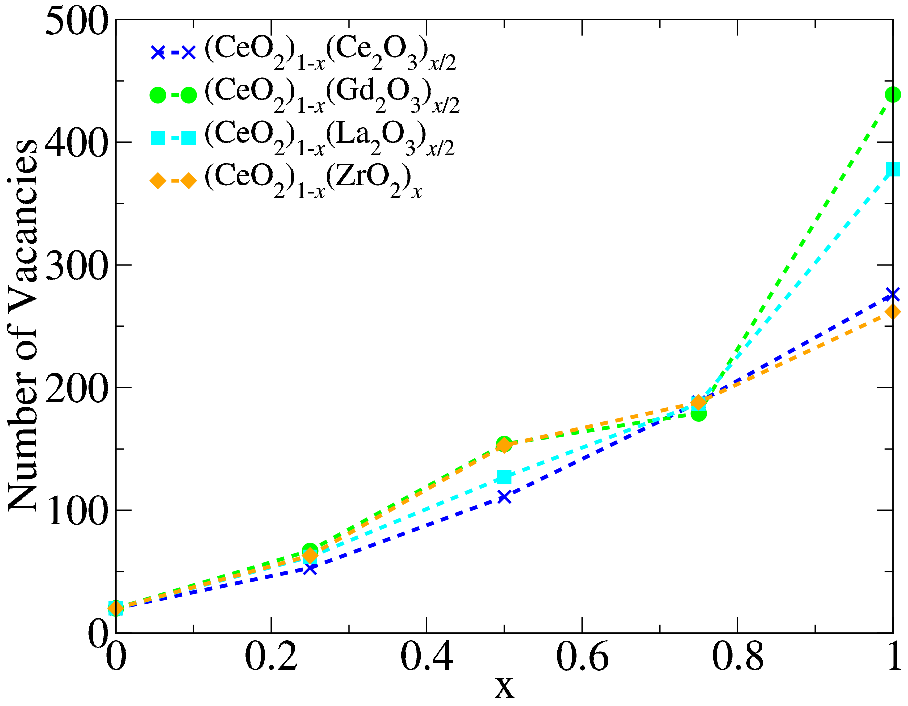

Figure S37: Dependency of the number of oxygen vacancies in the final structure on the relative concentration of the cation on mixed nanoparticles.

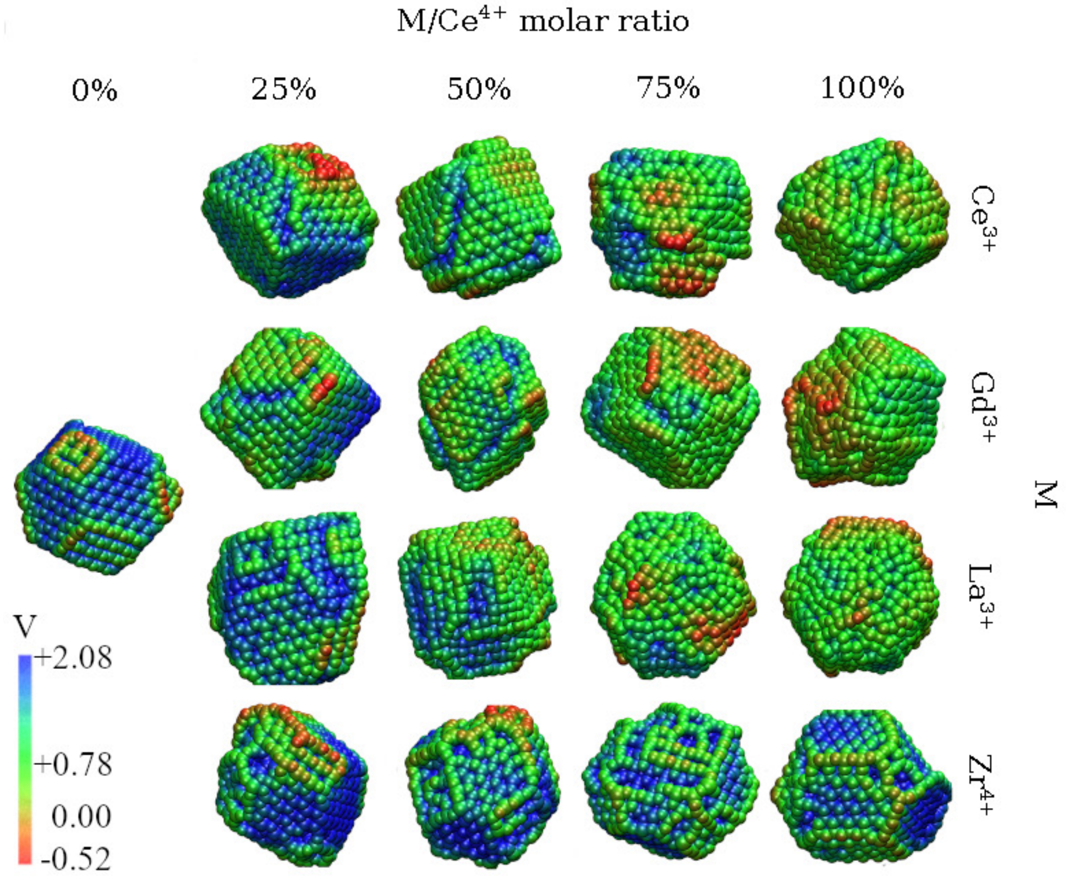

Figure S38: Map of electrostatic potential obtained with PME analysis for all nanoparticle structures at 0 K in relation to the M/Ce^{4+} ratio.

References

1 Sayle, D. C.; Feng, X.; Ding, Y.; Zhong, L. W.; Sayle, T. X. "Simulating synthesis": Ceria nanosphere self-assembly into nanorods and framework architectures. *J. Am. Chem. Soc.* **2007**, *129*, 7924–7935, DOI: `10.1021/ja070893w`.

2 Sayle, D. C.; Maicaneanu, S. A.; Watson, G. W. Atomistic models for CeO2(111), (110), and (100) nanoparticles, supported on yttrium-stabilized zirconia. *J. Am. Chem. Soc* **2002**, *124*, 11429–11439, DOI: `10.1021/ja020657f`.

3 Sayle, T. X. T.; Parker, S. C.; Sayle, D. C. Shape of CeO_2 nanoparticles using simulated amorphisation and recrystallisation. *Chem. Commun.* **2004**, *10*, 2438–2439, DOI: `10.1039/b408752f`.

4 Gražulis, S.; Chateigner, D.; Downs, R. T.; Yokochi, A. F. T.; Quirós, M.; Lutterotti, L.; Manakova, E.; Butkus, J.; Moeck, P.; Le Bail, A. Crystallography Open Database – Zn Open-Access Collection of Crystal Structures. *J. Appl. Crystallogr.* **2009**, *42*, 726–729, DOI: `10.1107/S0021889809016690`.

5 Gražulis, S.; Daškevič, A.; Merkys, A.; Chateigner, D.; Lutterotti, L.; Quirós, M.; Serebryanaya, N. R.; Moeck, P.; Downs, R. T.; Le Bail, A. Crystallography Open Database (COD): An Open-Access Collection of Crystal Structures and Platform for World-Wide Collaboration. *Nucleic Acids Res.* **2012**, *40*, D420–D427, DOI: `10.1093/nar/gkr900`.

6 Symington, A. R.; Molinari, M.; Moxon, S.; Flitcroft, J. M.; Sayle, D. C.; Parker, S. C. Strongly Bound Surface Water Affects the Shape Evolution of Cerium Oxide Nanoparticles. *J. Phys. Chem. C* **2020**, *124*, 3577–3588, DOI: `10.1021/acs.jpcc.9b09046`.

7 Seal, S.; Jeyaranjan, A.; Neal, C. J.; Kumar, U.; Sakthivel, T. S.; Sayle, D. C. Engineered Defects in Cerium Oxides: Tuning Chemical Reactivity for Biomedical, Environmental, & Energy Applications. *Nanoscale* **2020**, *12*, 6879–6899, DOI: `10.1039/D0NR01203C`.

8 Tabira, Y.; Withers, R. L.; Minervini, L.; Grimes, R. W. Systematic Structural Change in Selected Rare Earth Oxide Pyrochlores as Determined by Wide-Angle CBED and a Comparison with the Results of Atomistic Computer Simulation. *J. Solid State Chem.* **2000**, *153*, 16–25, DOI: `10.1006/jssc.2000.8712`.

9 Deori, K.; Gupta, D.; Saha, B.; Awasthi, S. K.; Deka, S. Introducing Nanocrystalline CeO_2 as Heterogeneous Environmental Friendly Catalyst for the Aerobic Oxidation of Para-Xylene to Terephthalic Acid in Water. *J. Mater. Chem. A* **2013**, *1*, 7091–7099, DOI: `10.1039/C3TA01590D`.

10 Patey, G.; Valleau, J. The Free Energy of Spheres with Dipoles: Monte Carlo with Multistage Sampling. *Chem. Phys. Lett.* **1973**, *21*, 297–300, DOI: `10.1016/0009-2614(73)80139-3`.

11 Torrie, G.; Valleau, J. Nonphysical Sampling Distributions in Monte Carlo Free-Energy

Estimation: Umbrella Sampling. *J. Comput. Phys.* **1977**, *23*, 187–199, DOI: `10.1016/0021-9991(77)90121-8`.

12 Kumar, S.; Rosenberg, J. M.; Bouzida, D.; Swendsen, R. H.; Kollman, P. A. THE Weighted Histogram Analysis Method for Free-Energy Calculations on Biomolecules. I. The Method. *J. Comp. Chem.* **1992**, *13*, 1011–1021, DOI: `10.1002/jcc.540130812`.